Journal of Magnetic Resonance **148,** 379–387 (2001)
doi:10.1006/jmre.2000.2264, available online at http://www.idealibrary.com on IDEAL®

Properties of the HYSCORE Spin Echo Signal

A. V. Astashkin*[,1,2] and A. M. Raitsimring†[,2]

*Institute of Chemical Kinetics and Combustion, Siberian Branch of Russian Academy of Sciences, 630090 Novosibirsk, Russia; and
†Department of Chemistry, University of Arizona, Tucson, Arizona 85721-0041

Received August 28, 2000; revised November 9, 2000

In hyperfine sublevel correlation spectroscopy (HYSCORE), the finite duration of the microwave pulses leads to an incomplete inversion of the electron spin magnetization by the third pulse, which results in a significant admixture of stimulated ESEEM to HYSCORE ESEEM. This virtually unavoidable contribution of stimulated ESEEM seriously hampers the analysis of the modulation amplitudes in HYSCORE. In this work, we analyze the properties of the spin echo signals contributing to the composite HYSCORE signal. Based on this analysis, we propose the strategies of HYSCORE data acquisition and processing that allow one to practically eliminate the contribution of the stimulated echo and make the HYSCORE ESEEM analyzable in quantitative terms.

Key Words: **ESE; ESEEM; HYSCORE; four-pulse echo; echo integration.**

INTRODUCTION

Two-dimensional (2D) hyperfine sublevel correlation (HYSCORE) spectroscopy introduced by Höfer *et al.* (*1*) is, undoubtedly, one of the most informative electron spin echo envelope modulation (ESEEM) techniques available today. A 2D spectrum obtained by the Fourier transformation (FT) of a HYSCORE ESEEM reveals correlations of nuclear transitions and disentangles contributions of different types of nuclei into the ESEEM. The HYSCORE method is based on the usual three-pulse (stimulated) ESE. The ESEEM frequency correlations are created by a sudden swapping of the electron spin manifolds during the time interval between the second and third microwave (mw) pulses of the stimulated ESE sequence. For this purpose, an additional mw pulse is used, counting third in the thus-obtained four-pulse sequence.

In ESE experiments, the mw pulses have finite durations and, correspondingly, a finite spectral range of their action on the electron spins. In HYSCORE, this leads to the incomplete inversion of the electron spin magnetization by the third pulse. As a result, the ESE signals of two types are simultaneously formed in the HYSCORE experiment (*2–6*). One of the signals is contributed by those spins reoriented by the third mw pulse. This is the signal of interest and the carrier of the HYSCORE ESEEM. The other signal, unwanted in this experiment, is the stimulated ESE, contributed by the spins whose orientation was not changed by the third pulse. This signal is a carrier of the stimulated ESEEM.

The HYSCORE and stimulated ESE signals cannot be separated by phase cycling (*4, 6*), and they both contribute to the resulting ESEEM. In the 2D spectrum, the stimulated ESEEM produces peaks on the main diagonal of the (++) quadrant, which may obscure the observation of weak HYSCORE lines located close to this diagonal. Even if this does not happen, the contribution of the stimulated ESE obliterates the reference for normalizing the HYSCORE modulation amplitudes and prohibits their simple analysis. Moreover, we as well as other researchers (*7*) have often observed that the amplitude of the HYSCORE echo is substantially less than that expected based on the probability of spin inversion by the third mw pulse. These observations imply that, besides the incomplete magnetization inversion, there are additional reasons for the loss of HYSCORE signal. Thus, the potential to provide information about the number of nuclei from the normalized modulation amplitudes remains unrealized in HYSCORE. This effectively limits the quantitative applications of this technique to the analysis of the ESEEM frequencies only.

In this work we show that the severe loss of the HYSCORE signal is caused by a somewhat different scale of response of the four-pulse and stimulated echoes to the electron-nuclear interactions. Based on our analysis, we propose the processing of the experimental data that allows one to obtain the pure HYSCORE ESEEM. The results of this work are also directly applicable to other one-dimensional (1D) and 2D experiments (*3, 5, 6, 8*) based on the same four-pulse sequence and differing in the incrementation schemes for the interpulse delays and in the types of spectral peaks obtained (fundamental, sum, or difference combination peaks and their various correlations).

EXPERIMENTAL

The experiments have been performed on homebuilt broadband pulsed EPR spectrometers operating at mw frequencies

[1] On leave to the Department of Chemistry, University of Arizona, Tucson, AZ 85721-0041.

[2] To whom correspondence should be addressed. Fax: (520) 621-8407. E-mail: andrei@u.arizona.edu.

1090-7807/01 $35.00

ranging from 2 to 8 GHz (*9*) and from 8 to 18 GHz (*10*). Each spectrometer has two independent mw channels. In the four-pulse ESEEM measurements we used the second mw channel to set the amplitude of the third pulse independently from the amplitudes of the other three pulses.

The data acquisition was performed using fast digitizing boards CS8500 from Gage Applied Sciences, Inc. (2-ns time resolution, 8-bit amplitude resolution, >200-MHz bandwidth, and about 15-kHz retriggering rate). The acquisition and storage of the whole ESE signal shape for every mw pulse separation have effectively added one more time dimension, the spin echo coordinate, to our experimental data. The measurements were performed with a pulse repetition rates of 500 Hz–1 kHz, limited by the saturation of the investigated samples.

The experiments were mostly performed with two types of well-characterized samples often used in a methodological pulsed EPR work. One of these samples, the γ-irradiated quartz, contains only a small fraction of magnetic nuclei ^{29}Si (4.67% natural abundance) and shows only a very weak ESEEM. The other sample was a 1 mM glassy methanol solution of 2,2,6,6-tetramethyl-1-piperidinyloxy (TEMPO) stable free radical obtained from Aldrich. In addition, a number of bioinorganic samples, e.g., sulfite oxidase and low-spin iron chlorine, were used.

RESULTS AND DISCUSSION

1. *The Four-Pulse ESE Signal in the Absence of Nuclear Interactions*

HYSCORE is essentially the nuclear coherence transfer experiment (*3, 5, 6, 8*) where ESEEM reflects the nuclear spin evolution between the mw pulses. However, the ESEEM is carried by the *electron* spin echo signal, whose amplitude is also determined by factors unrelated to the nuclei responsible for the ESEEM. If we narrow our scope down to the systems with the electronic spin $S = \frac{1}{2}$ and not too strongly anisotropic g-tensor, then the most important factor influencing the ESE amplitudes and shapes (apart from the ESEEM) is the width and shape of the EPR spectrum. In this section we wish to consider this factor separately, without complications associated with the ESEEM. The effects of the electron-nuclear interactions will be discussed in subsequent sections. Therefore, let us consider first the simplest spin system consisting of an electron spin $S = \frac{1}{2}$ and described by the spin-Hamiltonian, with only the Zeeman interaction taken into account:

$$\hat{H} = g\beta\hat{\mathbf{S}}\mathbf{B}_0, \qquad [1]$$

where g is the electronic g-factor, β is the Bohr magneton, and $\mathbf{B}_0$ is the external magnetic field.

The spin echo V_H generated by the four-pulse sequence θ_1–τ–θ_2–t_1–θ_3–t_2–θ_4–$(\tau + t')$, where θ_k is the nominal flip angle of the kth pulse and t' is the spin echo coordinate, can be readily evaluated using the formalism developed in Ref. (*11*) as

$$V_H = \int_{-\infty}^{\infty} \mathrm{Im}\{\alpha_1^*\beta_1^*\alpha_2^*\beta_2(|\alpha_3|^2 - |\beta_3|^2)\alpha_4\beta_4\exp(i\Delta\omega t')\} \times G(\Delta\omega)d(\Delta\omega). \qquad [2]$$

In this expression, $\Delta\omega$ is the difference between the electron Zeeman and the mw carrier frequencies, and $G(\Delta\omega)$ is the EPR spectrum shape. The α_k and β_k are

$$\alpha_k = \cos\frac{\omega_{Nk}t_{pk}}{2} - i\frac{\Delta\omega}{\omega_{Nk}}\sin\frac{\omega_{Nk}t_{pk}}{2};$$

$$\beta_k = -i\exp(i\varphi_k)\frac{\omega_{1k}}{\omega_{Nk}}\sin\frac{\omega_{Nk}t_{pk}}{2};$$

$$\omega_{Nk} = \sqrt{\omega_{1k}^2 + \Delta\omega^2}, \qquad [3]$$

where φ_k is the phase, t_{pk} is the duration, and ω_{1k} is the amplitude of the kth pulse. The latter two values determine the nominal flip angle $\theta_k = \omega_{1k}t_{pk}$.

The quantities $|\alpha_3|^2$ and $|\beta_3|^2$ represent the probabilities for the electron spins to be turned or not turned, respectively, by the third pulse (*11*). When the third pulse is "off," $|\alpha_3|^2 = 1$, $|\beta_3|^2 = 0$, and Eq. [2] describes the three-pulse stimulated echo signal $V_{SS}(t')$. In the opposite situation of the third mw pulse being "on," with $|\alpha_3|^2 = 0$ and $|\beta_3|^2 = 1$ for any $\Delta\omega$, the shape and the absolute value of the amplitude of $V_H(t')$ should be exactly same as those of $V_{SS}(t')$.

In a general case of $|\alpha_3|^2 \neq 0$, $|\beta_3|^2 \neq 0$, $V_H(t')$ is the sum of two terms:

$$V_H(t') = V_{HS}(t') + V_{HH}(t'). \qquad [4]$$

The term $V_{HH}(t')$, $(\propto|\beta_3|^2)$ is the signal of interest because, in the presence of the electron-nuclear interactions, it carries the HYSCORE ESEEM. The term $V_{HS}(t')$ $(\propto|\alpha_3|^2)$ is the unwanted stimulated echo generated in the four-pulse sequence. Below, the total V_H signal will be referred to as the composite echo, and the V_{HH} signal will be referred to as the HYSCORE or the four-pulse echo.

To give an idea about the shapes and relative amplitudes of V_{HH} and V_{HS}, we simulated these signals numerically, using Eqs. [2–4], for the mw pulses of equal durations and for the commonly used nominal flip angles θ_k of $\pi/2$, $\pi/2$, π, and $\pi/2$. The V_{SS} signal was simulated using the same expressions, with $t_{p3} = 0$ and $\theta_3 = 0$. The EPR line was assumed to be infinitely broad ($G(\Delta\omega) = 1$). The results of the simulations are shown in Fig. 1.

As seen from Fig. 1, for $G(\Delta\omega) = \mathrm{const}$ and for mw pulses of equal durations, the maximal amplitude $\tilde{V}_H$ of the composite

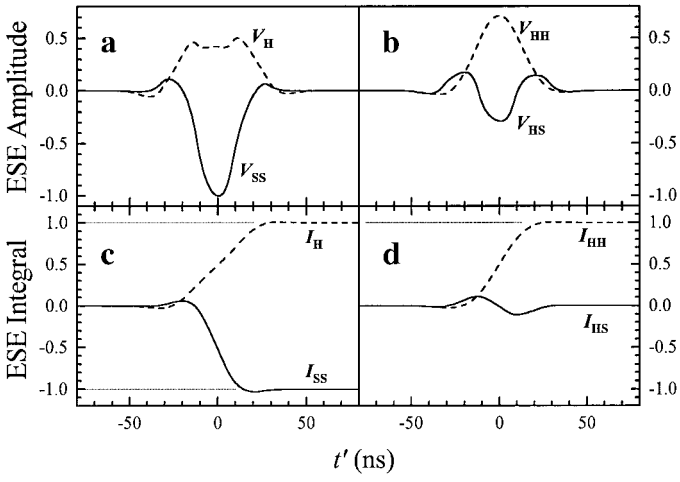

FIG. 1. (a) Simulated shapes of the three-pulse stimulated echo, V_{SS}, and the four-pulse composite echo, V_H. (b) Simulated shapes of the four-pulse stimulated echo, V_{HS}, and the four-pulse (HYSCORE) echo proper, V_{HH}, the latter two signals being the constituent parts of V_H. (c) and (d) Integrals of the ESE shapes shown in (a) and (b), respectively, over the spin echo coordinate t'. In the simulations, $t_p = 20$ ns for all pulses. The nominal flip angles in the calculation of V_{SS} were $\pi/2$ for all three pulses. In the calculation of V_{HH}, V_{HS}, and $V_H = V_{HH} + V_{HS}$, the nominal flip angles for the four pulses were $\pi/2$, $\pi/2$, π, and $\pi/2$. The EPR linewidth was taken to be infinite ($G(\Delta\omega) = \text{const}$). Note that the integral of V_{HS}, I_{HS} equals zero. The absolute values of the integrals of the composite echo ($|I_H|$), four-pulse echo ($|I_{HH}|$), and stimulated echo ($|I_{SS}|$) are equal.

echo is approximately half the maximal amplitude $\tilde{V}_{SS}$ of the three-pulse stimulated echo. The ratio $\tilde{V}_{HH}/\tilde{V}_{HS}$ (where the tilde denotes the absolute values of the maximal amplitudes of the respective ESE signals) is about 5:2, and so the composite signal contains about 30% of the unwanted signal. For an infinitely broad EPR spectrum, the ratio $\tilde{V}_{HH}/\tilde{V}_{HS}$ depends only on the relative durations of the mw pulses. As shown in Fig. 2, if the relative duration of the third mw pulse (with $\theta_3 = \pi$) decreases, the unwanted V_{HS} signal also decreases. This represents the most direct way to suppress the contribution of this signal to V_H (*6*).

Unfortunately, in the ESEEM applications, the implementation of such a direct approach is hindered by the limited power of the traveling wave tube amplifiers routinely employed in most ESE spectrometers, as well as by the necessity to use resonators with a low quality factor (to accommodate very short mw pulses), resulting in decreased sensitivity. We therefore chose to consider an alternative approach to eliminating the contribution of V_{HS} to V_H. This approach is based on the integral properties of ESE signals and may be more affordable than the "brute force" method discussed above (although it would also gain from the use of a possibly short third mw pulse).

Let us integrate $V_H(t')$ (Eq. [2]) over t'. Since $\int \exp(i\Delta\omega t')dt' \propto \delta(\Delta\omega)$ ("δ" is the delta-function), the integral over $\Delta\omega$ is readily evaluated:

$$I_H = \int_{-\infty}^{\infty} V_H(t')dt' = I_{HS} + I_{HH}$$

$$I_{HS} = \frac{\pi G(0)}{4} \sin\theta_1 \sin\theta_2 \cos^2\frac{\theta_3}{2} \sin\theta_4;$$

$$I_{HH} = -\frac{\pi G(0)}{4} \sin\theta_1 \sin\theta_2 \sin^2\frac{\theta_3}{2} \sin\theta_4, \qquad [5]$$

where I_{HS} is the integral of $V_{HS}(t')$, I_{HH} is the integral of $V_{HH}(t')$, and $G(0)$ is an amplitude of the EPR line at the observation position (i.e., at $\Delta\omega = 0$). Thus, in the integrated echo signal, the parameters related to the spin system ($G(0)$) and to the instrument (θ_k) are factorized.

One can see from Eq. [5] that $I_{HS} = 0$ if $\theta_3 = \pi$. At the same time, the integral of the HYSCORE echo, I_{HH}, becomes maximal and equal to the integral of the stimulated echo in the three-pulse sequence, I_{SS}, i.e., $|I_H(\theta_3 = \pi)| \equiv |I_{HH}(\theta_3 = \pi)| \equiv |I_{SS}|$. These integral properties are demonstrated in Figs. 1c and 1d. Despite the fact that so far we did not take the hyperfine (hfi) and nuclear quadrupole (nqi) interactions into account, we intend to consider here the possible use of these integral properties to eliminate the unwanted stimulated echo, $V_{HS}(t')$. Therefore, we will assume for the rest of this paper that $\theta_3 = \pi$, unless otherwise explicitly specified.

2. The Composite Spin Echo Signals Observed in Experiment and Their Qualitative Discussion

While experimenting with various systems at different mw bands (from S to P), we found that the conservation of integrals and the similarity of shapes of the experimental composite signals to those expected from simulations are often violated. Of the samples studied in this work, only the γ-irradiated quartz (at all operational frequencies) and TEMPO (at high

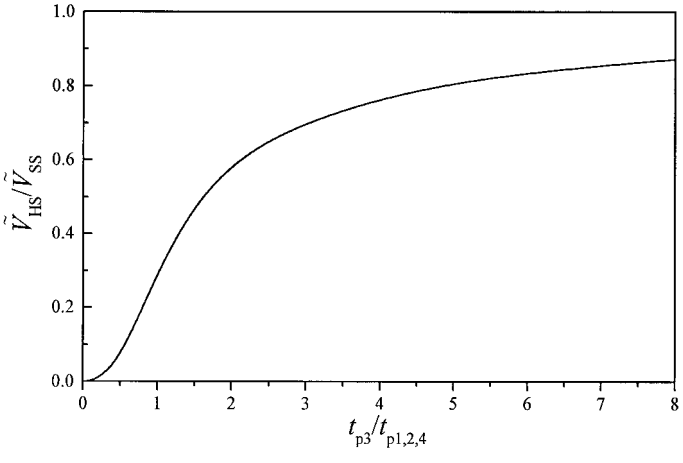

FIG. 2. Dependence of the ratio of amplitudes of stimulated echoes in four- and three-pulse sequences on the duration of the third pulse. The EPR linewidth is assumed to be infinite ($G(\Delta\omega) = \text{const}$).

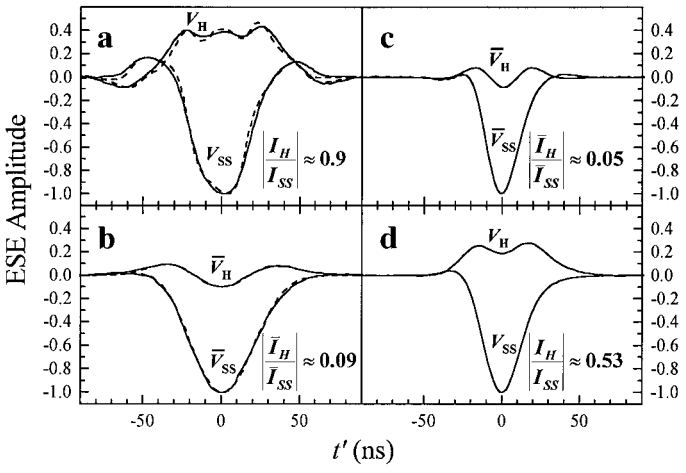

FIG. 3. Experimental and simulated shapes of three-pulse stimulated (V_{SS}) and four-pulse composite (V_H) echoes for various samples at various mw frequencies ν_{mw}. In all experiments, the nominal flip angles were $\pi/2$, $\pi/2$, and $\pi/2$ in the three-pulse sequence and $\pi/2$, $\pi/2$, π, and $\pi/2$ in the four-pulse sequence. The off-resonance baselines were subtracted from the ESE shapes. In (b) and (c) the averaging of the ESE shapes was performed after normalization by the nonoscillating part of the stimulated ESE decay. The ratios of ESE integrals are shown in all panels. (a) Solid lines: experimental for 1 mM solution of TEMPO in methanol at $\nu_{mw} = 16.375$ GHz, $B_0 = 585.5$ mT (maximum of the EPR spectrum), $\tau = 310$ ns, $t_1 = 1200$ ns, $t_2 = 2000$ ns; temperature, 77 K. All mw pulses were of 30 ns duration. Dashed lines: simulations using Eqs. [2–4] and the experimental EPR lineshape (for the stimulated ESE calculation, the third pulse in Eq. [2] was assumed to be off). (b) Solid lines: experimental for 1 mM solution of TEMPO in methanol at $\nu_{mw} = 3.758$ GHz, $B_0 = 134$ mT (maximum of the EPR spectrum), $\tau = 438$ ns; temperature, 20 K. All mw pulses were of 30 ns duration. The ESE shape $\bar{V}_H$ was obtained by averaging over all the individual shapes at different t_1 and t_2 of the 100×100 points HYSCORE data set. The shape $\bar{V}_{SS}$ was obtained by averaging over 200 points of the stimulated ESE data set. Dashed lines: simulations using the experimental EPR lineshape. The $\bar{V}_{SS}$ shape was simulated as in (a). The $\bar{V}_H$ shape was simulated using Eqs. [2, 3, 6] with α in Eq. [6] equal to 0.12 (which is close to $|\bar{I}_H/\bar{I}_{SS}| \cong 0.09$). (c) Low-spin *bis*-imidazole-d_4 complex of iron(III) tetraphenylchlorine at $\nu_{mw} = 16.652$ GHz, $B_0 = 500$ mT, $\tau = 400$ ns; temperature, 4.2 K. Microwave pulses were $3 \times$ (15 ns) in the three-pulse sequence and (15 ns) $\times$ (15 ns) $\times$ (10 ns) $\times$ (15 ns) in the four-pulse sequence. The ESE shape $\bar{V}_H$ was obtained by averaging over all the individual shapes at different t_1 and t_2 of the 80×80 point HYSCORE data set. The shape $\bar{V}_{SS}$ was obtained by averaging over 160 points of the stimulated ESE data set. (d) Mo(V) center in the high-pH form of sulfite oxidase at $\nu_{mw} = 15.795$ GHz, $B_0 = 571.5$ mT, $\tau = 400$ ns, $t_1 = 1300$ ns, $t_2 = 2500$ ns; temperature, 12 K. All mw pulses were of 20 ns duration.

operational frequencies) have produced results in agreement with the above simple theory. The experimental data for TEMPO at a high mw frequency are presented in Fig. 3a together with simulations based on Eqs. [2–4]. The integral I_H in this case is about 90% of I_{SS}, in good agreement with theory.

For other samples the I_H values were considerably smaller than I_{SS}. Because of deep ESEEM, the $V_H(t')$ shapes for these samples were different from those predicted by Eqs. [2–4] and strongly depended on time intervals between the mw pulses. In such situations, in order to minimize the distortions caused by ESEEM, the ESE signal shapes were averaged over the separations between the mw pulses. The averaged shapes and integrals are denoted by horizontal bars placed over the respective symbols (e.g., the ESE signal V_H averaged over t_1 and t_2 is denoted $\bar{V}_H$, and the integral of $\bar{V}_H$ over t' is denoted $\bar{I}_H$). Examples of cases significantly violating the conservation of integrals are presented in Figs. 3b–3d.

Although the shapes of the composite signals $\bar{V}_H$ in Figs. 3b–3d are very different from those predicted by Eqs. [2–4], we were able in all cases to reproduce the experimental shapes, using instead of Eq. [4] the expression with a weighted contribution of V_{HH}:

$$\bar{V}_H(t') = V_{HS}(t') + \alpha \cdot V_{HH}(t'), \qquad [6]$$

where α is a constant, and $V_{HS}(t')$ and $V_{HH}(t')$ are calculated using Eqs. [2, 3]. An example of such a simulation for TEMPO at low mw frequency is shown in Fig. 3b. We found that even in the worst cases of $|\bar{I}_H/\bar{I}_{SS}| < 0.1$, the value of α did not deviate from $|\bar{I}_H/\bar{I}_{SS}|$ by more than 30%. Phenomenologically, this result indicates that, for all investigated systems, the integral $\bar{I}_{HS}$ was close to zero. At the same time, the amplitude and integral of the HYSCORE signal V_{HH} were substantially smaller than the theoretical values. This absolute and relative loss of the HYSCORE signal, with the stimulated ESE signal remaining seemingly intact, requires an explanation and discussion.

Correlating the ESE and ESEEM data, one can notice that the loss of $\bar{I}_H$ is greater when a deep ESEEM is observed. If the modulation is shallow (like that in the γ-irradiated quartz or TEMPO at $\nu_{mw} = 16.375$ GHz), the ratio $|\bar{I}_H/\bar{I}_{SS}|$ is close to unity. Systematic measurements for TEMPO at different mw frequencies (the durations of the mw pulses were same in all measurements, and the nominal flip angles were $\theta_{1,2,4} = \pi/2$, $\theta_3 = \pi$) in order to vary the modulation amplitude show a regular decrease of $|\bar{I}_H/\bar{I}_{SS}|$ with decreasing ν_{mw} (see Fig. 4). At the same time, quite naturally for decreasing ν_{mw}, the ESEEM amplitude increases.

From these measurements we may conclude that the observed decrease of the V_{HH} signal relative to V_{HS} is caused by electron-nuclear interactions and has the same origin as the ESEEM. The ESE signal in the presence of ESEEM may be represented as the sum of oscillating and nonoscillating terms. In an orientationally disordered system, the oscillating components tend to damp, and the contributions of many different harmonics tend to cancel each other. Therefore, after a certain time interval between the mw pulses, the spin echo amplitudes approach their asymptotic values, different for the stimulated echo and HYSCORE. For example, in a system with $I = \frac{1}{2}$ (*2, 12*),

$$\tilde{V}_{SS}(\infty) \propto 1 - \frac{k}{2}; \quad \tilde{V}_{HH}(\infty) \propto 1 - \frac{3k}{4}, \qquad [7]$$

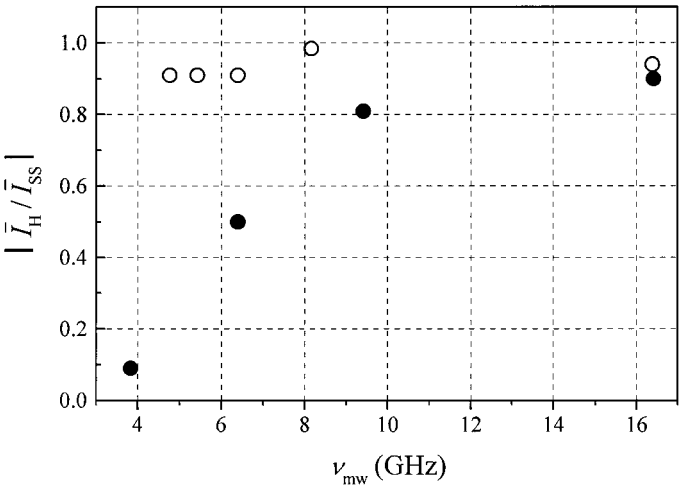

FIG. 4. Dependence of $|\bar{I}_H/\bar{I}_{SS}|$ on the mw frequency ν_{mw} for TEMPO (black circles) and γ-irradiated quartz samples (open circles). The data at $\nu_{mw} \sim 9.3$ GHz for TEMPO were collected using the pulsed EPR spectrometer of Professor Freed's research group. In the measurements of TEMPO, all of the mw pulses were 30 ns in duration. In the quartz measurements, the mw pulse durations were 100 ns (in order to make the excitation bandwidth narrower than the EPR spectrum width).

where k is the usual modulation amplitude factor (*12*), and the infinite arguments indicate that the separations between the mw pulses are large enough to ensure the complete damping of the ESEEM harmonics. If $k \ll 1$, the asymptotic amplitudes of both echoes are close to unity. In the opposite limit of $k \sim 1$, we have $\tilde{V}_{HH}(\infty)/\tilde{V}_{SS}(\infty) \sim 0.5$. Finally, if N nuclei with similar k values contribute to the ESEEM, a rough order-of-magnitude estimate of the asymptotic ESE amplitudes is given by

$$\tilde{V}_{SS}(\infty) \propto \left[1 - \frac{k}{2}\right]^N; \quad \tilde{V}_{HH}(\infty) \propto \left[1 - \frac{3k}{4}\right]^N. \qquad [8]$$

It follows from Eq. [8] that if $k \neq 0$ and N is large enough, the ratio of asymptotic amplitudes (and, possibly, the ratio of integrals $|\bar{I}_{HH}/\bar{I}_{SS}|$) may become arbitrarily small.

In our experiments, the average (over orientations) factor k for each of the close methyl protons of TEMPO was varied from about 0.02 at $\nu_{mw} = 16.4$ GHz to about 0.4 at $\nu_{mw} = 3.8$ GHz, as estimated for the anisotropic hfi constant $T_\perp \approx -3.5$ MHz (*13*). With 12 methyl protons, this gives $\tilde{V}_{HH}(\infty)/\tilde{V}_{SS}(\infty)$ changing from about 0.94 to about 0.2. In agreement with these estimates, the numerical calculation of the stimulated and four-pulse ESEEM traces for 12 methyl protons of TEMPO gives $\tilde{V}_{HH}/\tilde{V}_{SS} \cong 0.22$ for the low-frequency situation corresponding to Fig. 3b. The interaction of the electron spin with distant protons and with the hydrogen-bound hydroxyl protons of solvent (CH_3OH) (*12*) results in a further decrease of $\tilde{V}_{HH}/\tilde{V}_{SS}$.

The above estimates were made for $I = \frac{1}{2}$. For $I > \frac{1}{2}$ the results of the electron-nuclear interactions will be qualitatively the same, as demonstrated in Fig. 3c showing an example of data for such a system containing six strongly coupled ^{14}N nuclei.

Thus, a plausible reason for the loss of the HYSCORE signal is established. Other reasons, of minor importance, are discussed in Appendix I, while in Appendix II we discuss a possible application for this signal loss. It is, however, not clear yet how to separate V_H into its component signals, because the ESEEM behavior of V_{HS} is not known. Since V_{HS} is mostly contributed by nonresonant spins (at least for $\theta_3 = \pi$), its ESEEM might differ from that of V_{SS}. To explore this problem, direct numerical simulations are necessary.

3. Numerical Simulations in the Presence of Nuclear Interactions

Numerical simulations were performed for real mw pulses, using the density matrix formalism. Pulse propagators in these simulations were based on the full spin-Hamiltonian of the spin system ($S = \frac{1}{2}$, $I = \frac{1}{2}$), including electron and nuclear Zeeman interactions, hfi, and the interaction of the electron spins with the mw field. The desired signals were separated from the unwanted echoes by appropriate phase cycling (*2*). The V_{HS} and V_{HH} signals were calculated separately using diagonal and anti-diagonal blocks, respectively, of the third pulse propagator. All of the ESE signals were calculated as a function of two time variables. One of these variables was the spin echo coordinate t'. The other time coordinate for V_{SS} was the time interval T between the second and third mw pulses. In the four-pulse sequence, the second time coordinate was $t = t_1 = t_2$, which corresponds to the 1D combination peak (CP) experiment (*3*).

Some results of the calculations are presented in Fig. 5. In these particular simulations, the hfi parameters were similar to those for the methyl protons of TEMPO at the lowest ν_{mw} and B_0 used in our experiments. To maximize the ESEEM amplitude, the simulations were performed for the single crystal-like situation, with the angle θ between $\mathbf{B}_0$ and the axis of the hfi tensor equal to 45°. This resulted in the modulation amplitude factor $k \approx 0.7$. As seen in Fig. 5, the hfi practically did not change the shapes of $\bar{V}_{SS}$ and $\bar{V}_{HS}$ compared with the no-hfi case, resulting in $|\bar{I}_{HS}/\bar{I}_{SS}| \approx 0.002$. Both signals, however, decreased about 1.81 times as a result of the hyperfine interaction. Similarly, the shape of $\bar{V}_{HH}$ remained similar to that in the absence of hfi, but the amplitude of this signal decreased 3.36 times. The resulting ratios of the integrals are $|\bar{I}_{HH}/\bar{I}_{SS}| = |\bar{I}_H/\bar{I}_{SS}| \cong 0.55$. These changes of ESE amplitudes, with the shapes of the signals remaining unchanged, justify phenomenological Eq. [6]. The simulations with averaging over θ gave similar results, although the decrease of $|\bar{I}_H/\bar{I}_{SS}|$ was less pronounced in this case ($|\bar{I}_H/\bar{I}_{SS}| \approx 0.8$) due to smaller average modulation amplitude.

Simulation of the three- and four-pulse stimulated ESEEMs for various instrumental and hfi parameters (e.g., Fig. 6) re-

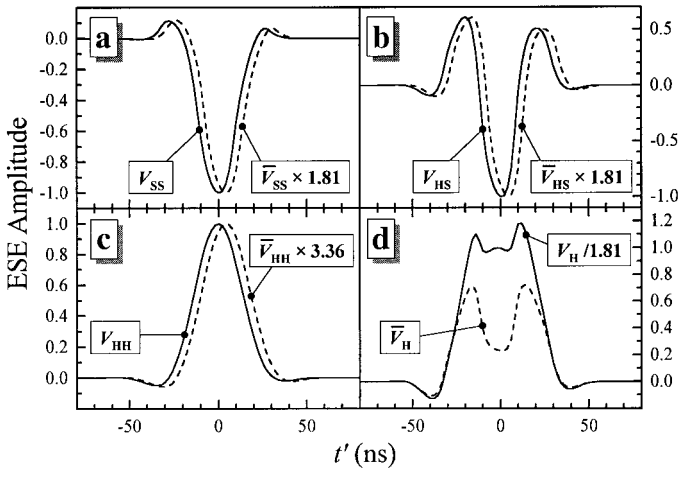

FIG. 5. Simulated shapes of three-pulse stimulated (a) and various four-pulse echoes (b–d) in the presence (dashed lines) and in the absence (solid lines) of electron-nuclear interaction. Simulation parameters: duration of all mw pulses, 20 ns; isotropic hfi constant $a_{iso} = 0$ MHz; $T_\perp = -4$ MHz; $\nu_I = 5.7$ MHz; $\tau = 200$ ns; the angle between $\mathbf{B}_0$ and the axis of the hfi tensor, $\theta = 45°$; average over 200 data points along T (for the three-pulse sequence) or $t = t_1 = t_2$ (for the four-pulse sequence). The scaling factors used to match the shapes simulated with and without hfi are shown. In (d) the shapes of composite echoes do not match because of different scaling factors for $\bar{V}_{HH}$ and $\bar{V}_{SS}$. The ESE shapes in (a–c) are shifted relative to each other by 4 ns. The ratio $|\bar{I}_H/\bar{I}_{SS}|$ in this case is equal to 0.55.

veals that the modulation patterns depend on t' in appearance, phase, and amplitude. In the vicinity of maxima of the ESE signals ($t' \approx 0$), however, the normalized ESEEMs and their FTs are quite close, as shown in Fig. 6c (this is only valid if amplitudes of the mw pulses exceed the Zeeman and hyperfine interactions, see Appendix III). Thus, at $t' \approx 0$, the ESEEM of the V_H signal can be represented as

$$\tilde{V}_H(t_1, t_2) = \frac{\tilde{\bar{V}}_{HS}}{\tilde{\bar{V}}_{SS}} \tilde{V}_{SS}(T) + \tilde{V}_{HH}(t_1, t_2), \qquad [9]$$

where $T = t_1 + t_2$. Equation [9] holds the key to eliminating the unwanted V_{HS} signal in the four-pulse experiments. Namely, the shapes of the three- and four-pulse stimulated echoes are to be simulated using Eqs. [2, 3]. These simulations allow one to determine $\tilde{\bar{V}}_{HS}/\tilde{\bar{V}}_{SS}$ because this ratio practically does not depend on the presence of ESEEM. Then, using the experimental $\tilde{V}_H(t_1, t_2)$ and $\tilde{V}_{SS}(T)$ (recorded at the same experimental conditions and, for $\tilde{V}_H(t_1, t_2)$, with $\theta_3 = \pi$) and the theoretical ratio $\tilde{\bar{V}}_{HS}/\tilde{\bar{V}}_{SS}$, the HYSCORE echo is separated using Eq. [9].

For processing the 1D data obtained in the four-pulse CP experiment (*3*), the stimulated echo $\tilde{V}_{SS}(T)$ should be recorded with the step in the third pulse interval, ΔT, being twice the step $\Delta t = \Delta t_1 = \Delta t_2$. Other 1D four-pulse experiments (*5*, *6*) will require different ΔT ($\Delta T = \Delta t_1$, $\Delta T = \Delta t_2$, or $\Delta T = 0$). For processing the 2D HYSCORE data of, say, $N \times N$ points, and with $\Delta t_1 = \Delta t_2$, one should record $2N - 1$ points of $\tilde{V}_{SS}(T)$, with $\Delta T = \Delta t_1 = \Delta t_2$, and convert them to the $N \times N$ 2D array in such a way that the element (i, j) of the output 2D array equals to the element $i + j - 1$ of the original 1D stimulated ESE data (here, $i, j \in [1 \cdots N]$). The described procedure allows one to obtain the HYSCORE spectra practically without any contribution from the stimulated ESEEM.

One example of such data processing is presented in Fig. 7. Figure 7a shows a HYSCORE spectrum of TEMPO obtained at a low mw frequency. The peaks in this spectrum located between two dashed anti-diagonal lines correspond to correlations of the fundamental harmonics. The peak at the proton Zeeman frequency, $\nu_I \cong 5.7$ MHz, is due to the distant protons, and the broad anti-diagonal ridge is due to the close methyl protons. All other features are the heteronuclear combination lines. Trace 1 in Fig. 7b represents a 1D projection of the portion of the 2D spectrum between the dashed lines. Trace 3 in Fig. 7b is the result of subtraction of the stimulated ESEEM using Eq. [9]. One can see that in this particular case the elimination of the V_{HS} signal resulted in a more than twofold increase of the Zeeman line due to distant protons.

A less rigorous but more simple way to suppress the unwanted V_{HS} signal is based on its integral properties and on the acquisition of $I_H(t)$ instead of $\tilde{V}_H(t)$. This method does not eliminate V_{HS} completely, because the ESEEM and signal amplitude are not factorized. As we have seen, however, the nonoscillating part of V_{HS} is practically eliminated by the

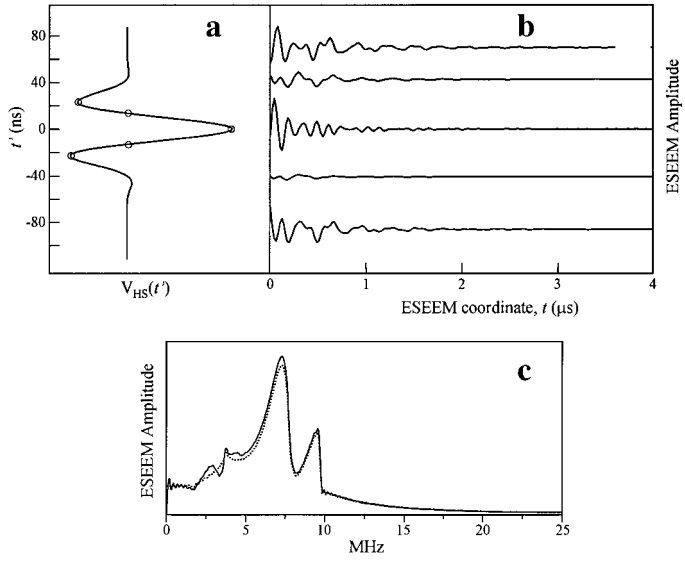

FIG. 6. (a) Simulated shape of the stimulated echo in the four-pulse sequence (V_{HS}) averaged over the time interval $t = t_1 = t_2$. (b) The ESEEM patterns observed at different points of this signal (marked by circles in (a) and arranged in the same order). (c) Amplitude FT spectra of the normalized modulations in the vicinity of the maxima (±4 ns) for the three-pulse stimulated echo V_{SS} (dots) and the four-pulse stimulated echo V_{HS} (solid line). Simulation parameters are as in Fig. 5, but the orientational averaging is performed.

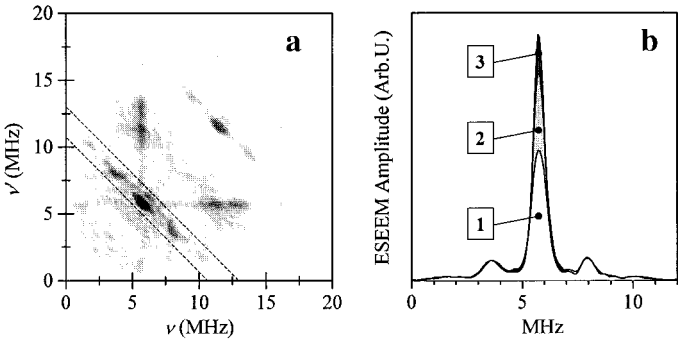

FIG. 7. (a) The (++) quadrant of the HYSCORE spectrum of TEMPO in methanol at $\nu_{mw} = 3.758$ GHz, $B_0 = 134$ mT (maximum of the EPR spectrum), $\tau = 438$ ns; temperature, 20 K. All mw pulses were of 30 ns duration. The ESE signal integration gate was 20 ns. (b) Trace 1: the 1D projection of the area between the dashed lines in the HYSCORE spectrum (a). Trace 3: the same, but after removing the contribution of the stimulated ESEEM as described in the text. Trace 2: the projection of the HYSCORE spectrum obtained with integration over the entire ESE signal (integration gate = 146 ns).

integration. The relative contribution of the stimulated ESEEM to I_H is also substantially suppressed, at least when the nuclei are far from the Zeeman/hfi cancellation condition. To avoid a loss of the desired modulation due to the phase dependence on t', the pulse duration in such an experiment should be shorter than the period of the modulation harmonic with the highest expected frequency. As an example, trace 2 in Fig. 7b shows the 1D projection of the HYSCORE spectrum obtained with the integration over the entire ESE signal. One can see that this spectrum is close to spectrum 3 obtained using Eq. [9], with the amplitude of the proton Zeeman line being about twice as great as that in spectrum 1.

CONCLUSION

In this work we investigated a structure and properties of the four-pulse ESE signal that is a carrier of the ESEEM in the four-pulse ESEEM experiments. We have explained the reasons for the loss of the amplitude of this signal often observed in experiments. We have proposed a rigorous way to eliminate the contribution of the unwanted stimulated ESE/ESEEM into the composite four-pulse signal and the use of the integrals of spin echo shapes for detecting "hidden" nuclei unobservable with standard ESEEM techniques. We have also proposed a more simple approximate way to eliminate the unwanted stimulated echo based on the integration of the ESE signal.

Since the suggested treatment of the four-pulse/HYSCORE experimental data is more complicated than that usually employed, we wish to make a final remark on its merits. In the case of weak ESEEM, one can easily suppress the stimulated ESE signal V_{HS} using the shortest possible third mw pulse and selecting durations for other pulses to be considerably longer than t_{p3} (*6*), while short enough to ensure the complete excitation of the ESEEM (*14*). For example, if there are only deuterium nuclei contributing to the ESEEM, one can select $t_{p3} = 10$ ns (close to the limits of modern hardware (*15*)) and $t_{p1} = t_{p2} = t_{p4} = 50$ ns, which will result in a practically zero contribution of V_{HS} (see Fig. 2). For weakly coupled protons in the X-band, however, the $\pi/2$ pulses should be no more than 15 ns long in order to provide for complete excitation of the ESEEM (*14*), which still results in a reasonable $\tilde{V}_{HS}/\tilde{V}_{HH} \cong 0.17$ for $t_{p3} = 10$ ns. In the case of very deep ESEEM, the suppression of V_{HS} with this straightforward technique may not be feasible, because the required durations for the $\pi/2$ pulses will be comparable with the transverse relaxation time in the sample (hundreds of nanoseconds). In such situations, the technique described in this work still allows one to eliminate the contribution of the stimulated echo to the composite HYSCORE signal, making this signal quantitatively analyzable in terms of the ESEEM amplitude.

APPENDIX I

Other Factors Influencing the Amplitude of the HYSCORE Echo

One of the factors that can affect the relative amplitude of V_{SS} and V_H signals (and the ratio of their integrals) is the relaxation caused by the instantaneous diffusion. A simple evaluation shows that for randomly distributed spins the decay caused by this mechanism is

$$V(\tau) \propto \exp\left(-8.1 \cdot 10^{-13} C\tau \left\langle 1 - \prod_k \cos \omega_{Nk} t_{pk} \right\rangle_{g(\omega)}\right), \quad [A1]$$

where C is the spin concentration in cm^{-3}, $\langle \cdots \rangle_{g(\omega)}$ indicates averaging over the EPR spectrum, and $k = 2, 3$ for stimulated echo (*16*) and 2, 3, 4 for HYSCORE. The ratio of the four-pulse and stimulated echo amplitudes due to the instantaneous diffusion mechanism is then

$$\frac{V_H}{V_{SS}} = \exp\left(-16.2 \cdot 10^{-13} C\tau \times \left\langle \cos \omega_{N2} t_{p2} \cos \omega_{N4} t_{p4} \sin^2 \frac{\omega_{N3} t_{p3}}{2} \right\rangle_{g(\omega)} \right), \quad [A2]$$

where it is taken into account that the third pulse of the stimulated ESE sequence is same as the fourth pulse of the four-pulse sequence, and pulse numbering corresponding to the four-pulse sequence is used. This ratio calculated for a 1 mM sample of TEMPO, $\tau \sim 400$ ns, and mw pulse durations of 20 ns (with the nominal flip angles of $\pi/2$, $\pi/2$, and $\pi/2$ for the stimulated echo, and $\pi/2$, $\pi/2$, π, and $\pi/2$ for the four-pulse echo) is not less than 0.96.

Another reason for the departures of the ESE signal shapes

and integrals from those predicted by the simple theory is the inhomogeneity of the mw field B_1 in a probe. Deviations from $\theta_3 = \pi$ result in an increase of V_{HS} and decrease of V_{HH} in the composite echo V_H. This effect is substantial only if the sample size is comparable with that of the resonator, and usually it can be easily avoided by decreasing the dimensions of the sample (unfortunately, for the samples of limited concentration this is not always an option). In our measurements, the samples were of cylindrical shape, having a height of approximately 5 mm and diameter of 3 mm. With samples of this size, even in the smallest resonator used with a height of 10 mm, the effect of B_1 inhomogeneity on the relative amplitudes of V_{HS} and V_{HH} does not exceed 10%, which is an order of magnitude less than that found in some of our measurements.

APPENDIX II

Detecting "Hidden Nuclei" with Four-Pulse ESE

As follows from numerical simulations (see Results and Discussion), the ratio $|\bar{I}_H/\bar{I}_{SS}|$ reflects the strength of the electron-nuclear interactions and the number of the interacting nuclei (see Eq. [8]). Normally, these nuclei can be studied using the ESEEM spectra. However, if the nuclei have rather strong hfi with distributed parameters (e.g., due to slightly different conformations of the paramagnetic center), they might become practically undetectable with conventional ESEEM methods because the corresponding ESEEM harmonics will damp within the dead time. The nonoscillating term of the ESEEM, on the other hand, always adds up constructively, leading to the decrease of the average (over the time intervals) echo amplitude. As our analysis shows, the presence of such "invisible" nuclei may be established if the deviation of $|\bar{I}_H/\bar{I}_{SS}|$ from unity is considerably greater than that predicted based on the nuclear parameters obtained from the observable ESEEM.

Such a situation was found, e.g., in a sample of the high pH form of sulfite oxidase that contains a paramagnetic Mo(V) center coordinated by the OH_2 group (*17, 18*). The anisotropic hfi of the close hydroxyl protons is quite strong and distributed in broad limits (*18*), so that it has taken considerable effort and application of the zero dead time refocused primary ESE technique (*13*) in combination with low mw frequency to detect them at all. At the same time, the measurement of the integrals of the composite and stimulated echoes, at $\nu_{mw} \sim 16$ GHz, gives $|\bar{I}_H/\bar{I}_{SS}| \approx 0.53$, indicating the presence of close protons in vicinity of the Mo(V) center.

APPENDIX III

Half-Frequency Harmonics in the Four-Pulse Stimulated ESEEM

The numerical simulations have revealed some peculiarities of the stimulated ESEEM as obtained with the four-pulse sequence, which are related to the nuclear spin evolution during the mw pulses. Figure 8 shows the simulated spectra of the three- and four-pulse stimulated ESEEMs for a single $I = \frac{1}{2}$ nucleus with $\nu_I = 8$ MHz and $T_\perp = -5$ MHz. The magnetic field $\mathbf{B}_0$ was oriented at the "magic angle" (54.7°) with respect to the hfi axis. In this case the nuclear transition frequencies are degenerate, $\nu_\alpha = \nu_\beta \approx \nu_I$. Therefore, only one line should be observed in the stimulated ESEEM spectra, with the frequency close to ν_I.

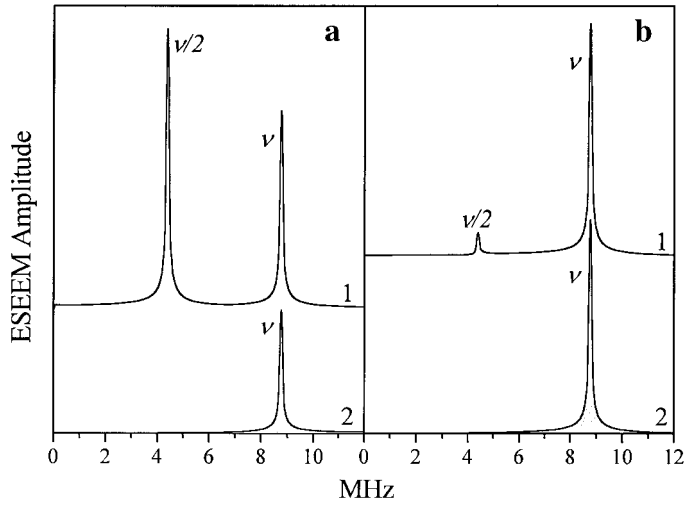

FIG. 8. Traces 1 and 2 in both panels: the amplitude spectra of normalized four-pulse (1D) and three-pulse stimulated ESEEM, respectively, calculated for mw pulse durations of 30 ns in (a) and 10 ns in (b). The simulation parameters were $S = \frac{1}{2}$, $I = \frac{1}{2}$, $\nu_I = 8$ MHz, $a_{iso} = 0$ MHz, $T_\perp = -5$ MHz, $\tau = 200$ ns. The angle θ between $\mathbf{B}_0$ and the hfi axis is 54.7°. The peak labeled "ν" results from the usual fundamental harmonics (at $\theta = 54.7°$ they have similar frequencies). The peak labeled "$\nu/2$" in trace 1 results from the nuclear spin evolution during the third mw pulse (see text).

Indeed, the spectra of the three-pulse stimulated ESEEM (traces 2 in Figs. 8a and 8b) show only one line at the frequency $\nu = \nu_\alpha = \nu_\beta \cong 8.75$ MHz. An additional line, however, is present in the spectra of the four-pulse stimulated ESEEM (trace 1 in Figs. 8a and 8b), with the frequency $\nu/2 = \nu_\alpha/2 = \nu_\beta/2 \cong 4.38$ MHz. The latter harmonic appears in the four-pulse stimulated ESEEM because the third pulse *of finite duration* has a probability of turning the electron spin by the angle of $n \times 2\pi$ ($n \neq 0$), accompanied by the turn of the nuclear spin (same as it occurs in pulse-adjustable and pulse-matched ESEEM (*19–21*) and coherent Raman beats (*22*) techniques). Such a flip results in termination of the nuclear coherences already evolving after the second pulse and in starting the new coherences, which leads to the harmonics in the four-pulse stimulated ESEEM described by $\cos(\omega_{\alpha(\beta)} t_{1(2)} + \omega_{\alpha(\beta)}\tau/2)$. There are similar harmonics in the four-pulse ESEEM proper (*2*). In the latter case, however, they can appear without any nuclear spin evolution during the mw pulse, since the nuclear coherences are transferred between the electron spin manifolds with different sets of nuclear eigenfunctions (*5, 6*).

During the time interval between the second and fourth pulses, the terminated coherences acquire the phase $\varphi_1 = \nu t_1$, and those newly created acquire the phase $\varphi_2 = \nu t_2$, where ν is the frequency of the nuclear transition. In stimulated ESE, we measure the phase of the nuclear coherences as a function of $T = t_1 + t_2$. The above phases may then be rewritten as $\varphi_1 = (\nu t_1/T) \cdot T$ and $\varphi_2 = (\nu t_2/T) \cdot T$, showing that the frequencies of the corresponding oscillations observed in the FT spectra are $\nu t_1/T$ and $\nu t_2/T$. In the 1D four-pulse (CP) experiment, $t_1 = t_2 = T/2$ and these frequencies are equal to $\nu/2$. In the 2D HYSCORE spectra these harmonics will give peaks along the frequency axes (i.e., at $\nu_{1(2)} = 0$; $\nu_{2(1)} \neq 0$), although in practice these peaks are usually suppressed by the preliminary data processing that includes the subtraction of the nonoscillating component from the time domain data.

As expected, the relative amplitude of the $\nu/2$ line(s) in four-pulse stimulated ESEEM spectra decreases when the mw pulses become sufficiently short and strong, with their amplitude (in frequency units) considerably exceeding the nuclear transition frequencies (compare traces 1 in Figs. 8a and 8b). Besides, upon increasing the amplitude of the mw pulses, the amplitude of the "normal" line at frequency ν becomes similar to that in usual three-pulse stimulated ESEEM (compare traces 1 and 2 in Fig. 8b). The latter circumstance was used in this work for eliminating the contribution of the stimulated ESEEM to the composite ESEEM observed with the HYSCORE technique.

ACKNOWLEDGMENTS

Preliminary experiments on the investigation of properties of the HYSCORE echo were performed using the X-band instrument of the research group of Prof. J. Freed. A.R. is very grateful to Prof. Freed for the kind permission to perform these experiments and for numerous discussions. He is also grateful to P. Borbat for his invaluable assistance in these experiments. The financial support of NSF BIR-9224431 and DBI-9604939 is warmly acknowledged.

REFERENCES

1. P. Höfer, A. Grupp, H. Nebenführ, and A. Mehring, *Chem. Phys. Lett.* **132,** 279 (1986).
2. C. Gemperle, G. Aebli, A. Schweiger, and R. R. Ernst, *J. Magn. Reson.* **88,** 241 (1990).
3. A. Schweiger, *Angew. Chem. Int. Ed. Engl.* **30,** 265 (1991).
4. J. J. Shane, "Electron Spin Echo Envelope Modulation Spectroscopy of Disordered Solids," Ph.D. Thesis, Nijmegen, 1993.
5. A. Ponti and A. Schweiger, *J. Chem. Phys.* **102,** 5207 (1995).
6. M. Hubrich, G. Jeschke, and A. Schweiger, *J. Chem. Phys.* **104,** 2172 (1996).
7. M. K. Bowman, private communications; P. Höfer, private communications.
8. S. Van Doorslaer and A. Schweiger, *Chem. Phys. Lett.* **281,** 297 (1997).
9. A. V. Astashkin, V. Kozlyuk, and A. M. Raitsimring, *in* "Abstracts of the 40th Rocky Mountain Conference on Analytical Chemistry," Denver, CO, July 26–30, 1998, additional materials.
10. P. P. Borbat and A. M. Raitsimring, *in* "Abstracts of the 36th Rocky Mountain Conference on Analytical Chemistry," p. 94, Denver, CO, July 31–August 5, 1994.
11. A. Bloom, *Phys. Rev.* **98,** 1105 (1955).
12. S. A. Dikanov and Yu. D. Tsvetkov, "Electron Spin Echo Envelope Modulation (ESEEM) Spectroscopy," CRC Press, Boca Raton, FL, 1992.
13. A. V. Astashkin and A. M. Raitsimring, *J. Magn. Reson.* **143,** 280 (2000).
14. A. V. Astashkin, S. A. Dikanov, V. V. Kurshev, and Yu. D. Tsvetkov, *Chem. Phys. Lett.* **136,** 335 (1987).
15. P. P. Borbat, R. H. Crepeau, and J. H. Freed, *J. Magn. Reson.* **127,** 155 (1997).
16. K. M. Salikhov, A. M. Raitsimring, and S. A. Dzuba, *J. Magn. Reson.* **42,** 25 (1981).
17. A. M. Raitsimring, A. Pacheco, and J. H. Enemark, *J. Am. Chem. Soc.* **120,** 11263 (1998).
18. A. V. Astashkin, M. L. Mader, A. Pacheco, J. H. Enemark, and A. Raitsimring, *J. Am. Chem. Soc.* **122,** 5294 (2000).
19. V. V. Kurshev, A. V. Astashkin, and A. M. Raitsimring, *J. Struct. Chem.* **29,** 62 (1988).
20. A. Raitsimring, D. H. Crepeau, and J. H. Freed, *J. Chem. Phys.* **102,** 8746 (1995).
21. G. Jeschke, R. Rakhmatullin, and A. Schweiger, *J. Magn. Reson.* **131,** 261 (1998).
22. M. K. Bowman, *Isr. J. Chem.* **32,** 339 (1992).